AIAA 81-0275R

# Aerodynamic Interaction of Heat Transfer with Steady Transonic Flow

M. Kurosaka,* H. Kuroda,† H. P. Chou,‡ and J. M. Wu§
*The University of Tennessee Space Institute, Tullahoma, Tenn.*

**In the design of turbine stages, the transonic flowfield between the blades is usually calculated under the assumption of an insulated wall. However, the heat and mass transfer induced by the turbine cooling may exert a first-order effect upon the sensitive transonic flowfield and alter it significantly from the thermally insulated and zero mass-transfer condition. In this paper, attention has been focused on the effect of heat transfer only; an experimental study has been conducted to investigate the interactive effect between the heat transfer and the steady transonic flow in a simple convergent-divergent duct. The results show that the position of the shock is considerably affected by the effect of wall cooling. The physical explanation for the shift is also offered. The results may have implications in the other internal flow problems.**

## Nomenclature

$A$ = cross-sectional area of a duct
$c_p$ = specific heat at constant pressure
$h$ = nozzle throat height
$K$ = acceleration parameter, $(\mu_e/\rho_e)(1/u_e^2)(du_e/dx)$
$p$ = static pressure
$p_e$ = exhaust static pressure, measured at 21.3 mm (8.4 in.) from throat
$p_t$ = total pressure at settling chamber
$T$ = static temperature
$T_t$ = total temperature at settling chamber
$T_w$ = wall temperature at throat
$u$ = velocity in the $x$ direction
$u_\tau$ = frictional velocity $(\tau_w/\rho_w)^{1/2}$
$x$ = distance measured from the throat along the duct
$x_s$ = position of shock measured from the throat
$y$ = vertical distance from wall
$\Delta$ = difference
$\delta^*$ = displacement thickness, $\int_0^{h(x)/2} [1-(\rho/\rho_e)(u/u_e)]\,dy$
$\rho$ = density
$\mu$ = viscosity
$\tau_w$ = wall shear stress

*Subscripts*

$e$ = condition at freestream edge of boundary layer
$w$ = wall condition
$1$ = just upstream of shock

## Introduction

THE advance in turbine design has steadily enabled the engine manufacturers to push toward higher stage loading and Mach number than traditionally possible, resulting in fewer stages; a well-known example is the F404 turbofan engine, where the high- and low-pressure turbines each consist of a single stage.

Needless to say, such a trend makes it imperative to minimize assorted losses. As the turbine stator exit velocity becomes supersonic, the shock losses in particular assume increasing importance.

Figure 1 shows schematically the pattern of shock waves and a sonic line between the stators with supersonic exit velocity. The accurate prediction of the sonic line and shock pattern in design is of obvious importance for the estimate of flow ingestion capability, stage loading, and shock losses.

In current design practice, the sonic line and shock patterns are usually predicted by the blade-to-blade or cascade flow analysis; the state-of-the-art methods within the framework of inviscid adiabatic flow are described by Gopalakrishnan and Bozzola,[1,2] McDonald,[3] Delaney and Kavanaugh,[4] and Ives and Liutermoza.[5] The effect of the boundary layer upon the inviscid flow is discussed by Gliebe.[6] However, the boundary-layer calculation method adopted therein is restricted to an insulated wall; therefore, it is not indiscriminately applicable to cooled turbine blades, although certainly appropriate in the context of flow through fans and compressors, as intended in Ref. 6.

In the flow passage of a cooled turbine, the heat and mass transfer caused by wall cooling and coolant injection may significantly interfere with the steady flowfield and markedly alter the sensitive transonic flow regime in particular. (By contrast, for the subsonic regime, such an effect is expected to be small, as postulated by Hartsel[7]; this point was confirmed, though indirectly, in a series of efficiency data.[8-12]) Even when we restrict our attention to the inviscid core outside of the boundary layers, a simplified, one-dimensional analysis[13] displays a well-known and important influence of heat and mass transfer upon the transonic flow; the effect may be as influential as a change in the cross-sectional area. In the turbine transonic flow, the response of the boundary layer to

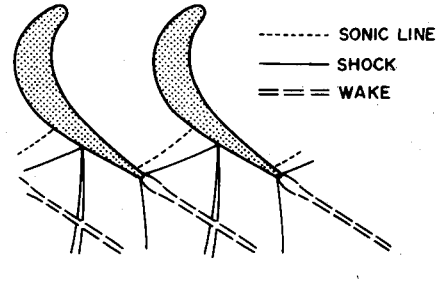


**Fig. 1 Flow pattern in transonic turbine passage.**

Presented as Paper 81-0275 at the AIAA 19th Aerospace Sciences Meeting, Jan. 12-15, 1981; submitted Feb. 20, 1981; revision received Aug. 11, 1981. 

*Professor of Aerospace and Mechanical Engineering. Associate Fellow AIAA.
†Graduate Student. Student Member AIAA.
‡Research Engineer presently with AVCO Everett Research Laboratories, Everett, Mass.
§Professor of Aerospace Engineering. Associate Fellow AIAA.

the effect of heat and mass transfer may become amplified to a sizeable extent.

In spite of the expected importance of the interactive effects of heat and mass transfer on the transonic turbine stage, the only published work known to the present authors is that of Studerus[14]; he examined the effect of mass transfer due to coolant injection to the mainstream—in the framework of inviscid flow—by modifying the normal component of velocity on the airfoil surface to nonzero values. Therefore, not only the effect of heat transfer but also the behavioral change of the boundary layer and its resulting influence upon the pressure distributions are outside the scope of Ref. 7.

In view of this, the present investigation is aimed at a study of the interactive effects of heat and mass transfer upon the transonic flowfield. It is deemed advantageous to separate initially the effects of heat and mass transfer and then later combine them together. This paper deals with the effect of heat transfer only, the next phase being intended for the influence of mass transfer and the combined effects.

To achieve our stated objective in a simplified environment devoid of geometrical complexity, a convergent-divergent nozzle representative of a turbine passage has been chosen as a test section, where the effect of cooling upon the steady transonic flowfield has been investigated.

Aside from its implications directly related to turbomachinery, such an investigation into the interactive effect of heat transfer appears to be of interest in its own right.

## Experimental Apparatus and Instrumentation

The contour of the convergent-divergent duct, shown in Fig. 2, is selected to simulate approximately the area change in a typical turbine flow passage between stator blades. The throat has a height of 22.9 mm (0.9 in.) and a width of 203 mm (8 in.), the rectangular cross section being chosen to represent the two-dimensional, cascade flow condition. The area contraction ratio upstream of the throat is 8.19, while the area expansion ratio downstream of it is 2.06. The contoured walls, forming the top and bottom walls of the convergent-divergent nozzle, are made of copper and cooled by water circulating through the jacket which surrounds the nozzle; the back pressure in the convergent-divergent duct is controlled by two pressure control flaps.

The entire test rig is shown in Fig. 3. The high-pressure air stored in a separate tank is fed to a combustor through pressure regulators. The combustor is a can type used for J-79 engines; portions of its original airholes have been closed off to make the combustor suitable for the operation at reduced flow rate [maximum 2.9 kg/s (6.3 lbm/s)]; the air at maximum 35.9 Pa (52 psia) is heated up to 760°C (1400°F) by combustion with kerosene, which is ignited by a furnace-type igniter.

After the combustor, the air at elevated temperature passes through an octagonally shaped diffuser and a settling chamber. Inserted within the settling chamber to eliminate the flow distortion are three wire mesh screens. To avoid the direct contact of hot air with the structural members, the internal surfaces of both the diffuser and the settling chamber are coated with refractory shield material; aluminum-oxide clay of 25 mm (1 in.) thickness. This is followed by the water-cooled test section; to allow flow visualization, the side walls of the test section are equipped with heat-resistant optical glass of 6.35 mm (0.25 in.) thickness (Corning VYCOR 7913).

Static pressure taps nominally 5.1 mm (0.2 in.) apart in the flow direction, 60 on top and 60 on bottom walls of the test section, are provided. The pressure at 213 mm (8.4 in.) from the throat, a point closest to the exhaust, is taken here as the exhaust pressure, denoted as $p_e$. The window with optical glass may be replaced with steel side plates, where static pressure can be measured at 115 locations. The pressure taps are scanned by Scannivalve 48J9-1. Five Chromel-Alumel thermocouples, 50.8 mm (2 in.) apart in the flow direction, are embedded in the wall surfaces and scanned by a Fluke 2024A scanner; the temperature measured by the thermocouple located at the throat is denoted as $T_w$ and used as a reference value, the maximum deviation among the readings of the thermocouples being 6°C (11°F). A microprocessor controls various aspects of the experiment.

A standard two-mirror schlieren system is used to locate the shock position. The velocity profiles of the boundary layer are measured by total pressure probes.

Figure 4 shows a view of the entire test facility.

## Experimental Results

Figures 5-7 display the observed changes in the shock position due to the effect of wall cooling; in all of them the

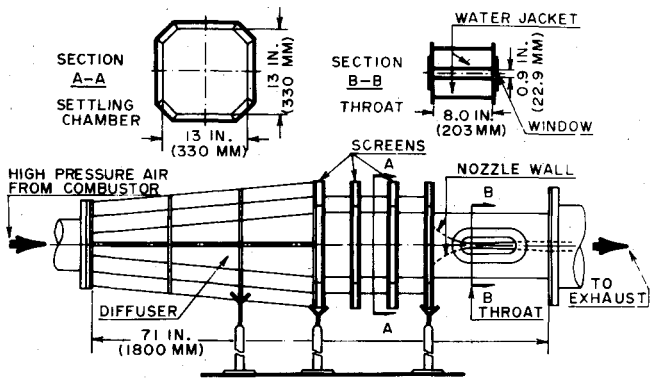


Fig. 3 Test rig layout.

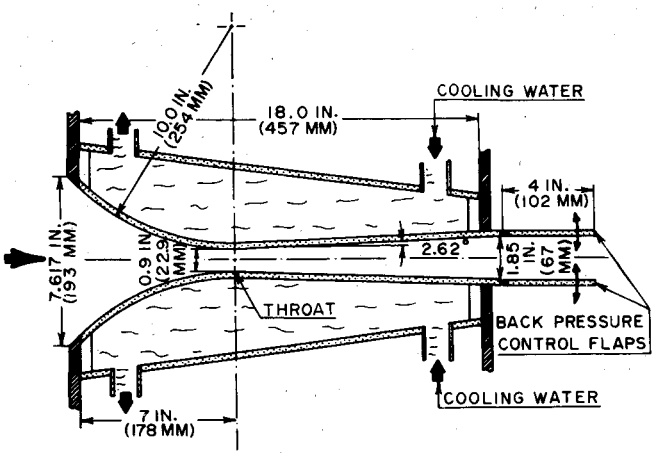


Fig. 2 Convergent-divergent nozzle.

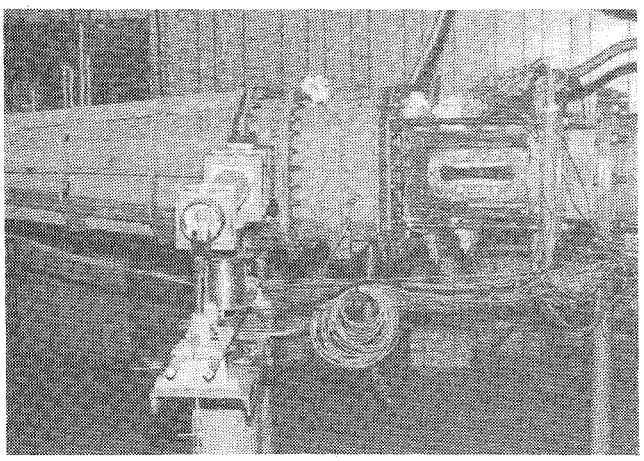

Fig. 4 View of test facility.

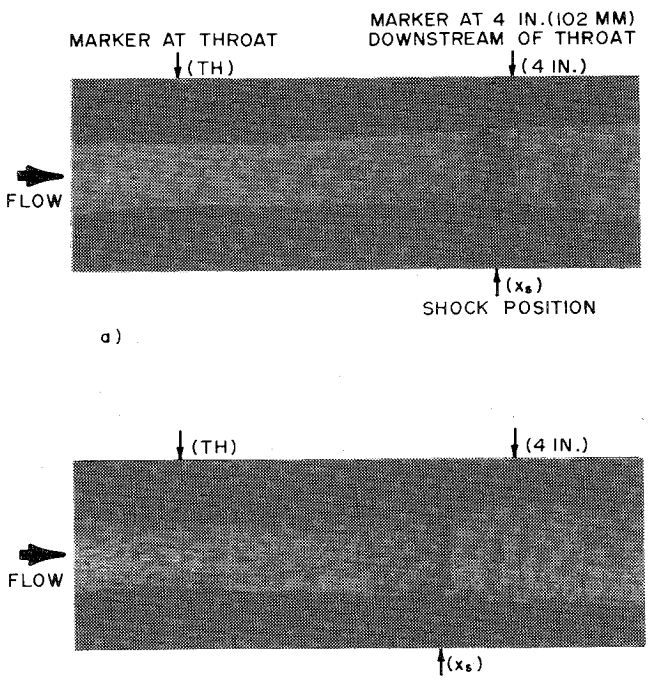


**Fig. 5** a) $p_e/p_t = 0.597$, $T_w/T_t = 0.498$, $x_s/h = 4.24$ with cooling; b) $p_e/p_t = 0.595$, $T_w/T_t = 0.652$, $x_s/h = 3.47$ without cooling.

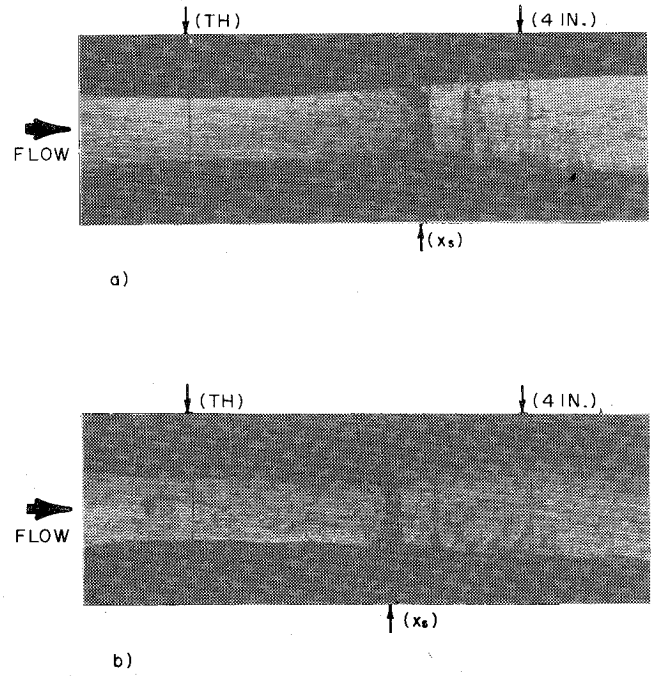


**Fig. 6** a) $p_e/p_t = 0.663$, $T_w/T_t = 0.461$, $x_s/h = 3.07$ with cooling; b) $p_e/p_t = 0.669$, $T_w/T_t = 0.685$, $x_s/h = 2.62$ without cooling.

position of the back pressure control flap is held constant, approximately 2 deg inward; the data are all taken at hot runs where combustion is taking place, flow conditions being given in Table 1. In these figures, the direction of flow is from left to right. Two vertical lines are markers, one located at the throat and the other at 102 mm (4 in.) downstream of it.

Figure 5 corresponds to the low-pressure ratio of $p_e/p_t = 0.6$. By comparing Fig. 5a (with cooling) with Fig. 5b (without cooling), one observes that the effect of wall cooling

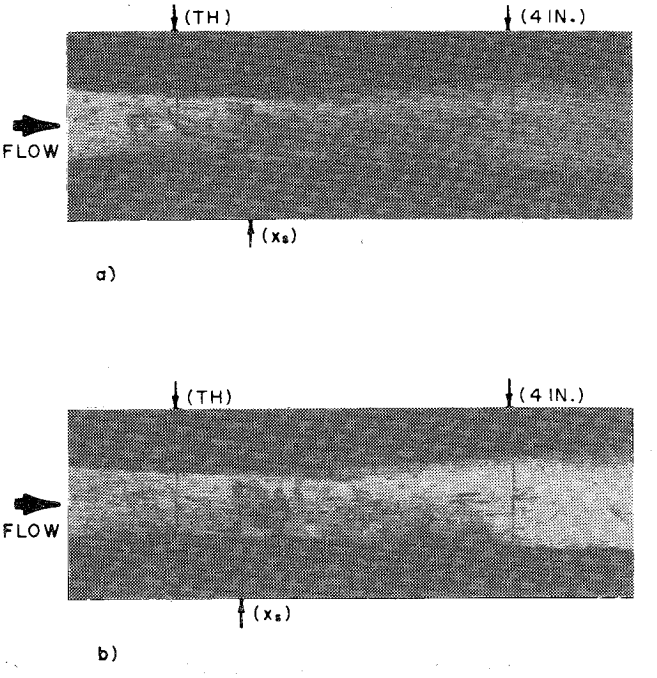


**Fig. 7** a) $p_e/p_t = 0.800$, $T_w/T_t = 0.461$, $x_s/h = 0.98$ with cooling; b) $p_e/p_t = 0.800$, $T_w/T_t = 0.672$, $x_s/h = 0.95$ without cooling.

**Table 1 Flow conditions**

| Fig. | Condition | $p_t$, Pa (psia) | $p_e$, Pa (psia) | $T_t$, K (°R) | $T_w$, K (°R) |
|---|---|---|---|---|---|
| 5a | With cooling | 17.8 (25.8) | 10.6 (15.4) | 671.0 (1207.8) | 334.2 (601.5) |
| 5b | Without cooling | 17.6 (25.5) | 10.5 (15.2) | 641.7 (1155.0) | 418.4 (753.1) |
| 6a | With cooling | 15.7 (22.8) | 10.4 (15.1) | 662.1 (1191.7) | 305.2 (549.4) |
| 6b | Without cooling | 15.4 (22.4) | 10.3 (15.0) | 776.0 (1396.8) | 531.6 (956.8) |
| 7a | With cooling | 13.1 (19.0) | 10.5 (15.2) | 824.4 (1484.0) | 380.1 (684.1) |
| 7b | Without cooling | 12.7 (18.4) | 10.1 (14.7) | 773.7 (1392.7) | 519.9 (935.9) |

shifts the position of the shock in the downstream direction; the amount of movement measured at the nozzle centerline is $\Delta(x_s/h) = 4.24 - 3.47 = 0.77$ [in the actual dimension, this corresponds to $\Delta x_s = 17.6$ mm (0.69 in.)].

As $p_e/p_t$ is raised, the shock moves upstream, as expected. At the same time, the shift in the shock position becomes less; in Fig. 6, which corresponds to $p_e/p_t = 0.66$, the shock movement due to cooling is $\Delta(x_s/h) = 0.45$; in Fig. 7 for $p_e/p_t = 0.80$, $\Delta(x_s/h) = 0.03$.

Figure 8 summarizes these observed shifts in the shock position, including the results of other flow conditions and various positions of the back pressure control flap. The degree of wall cooling is categorized in the following six ranges: $T_w/T_t = 0.3$-0.4, 0.4-0.5, 0.5-0.6, 0.6-0.7, 0.7-0.8, and above 0.8, the last corresponding to the cold runs (without combustion). The two straight lines represent the least square fit curves in two separate ranges of $T_w/T_t$. Observe again that the shift in the shock position due to cooling increases as $p_e/p_t$ decreases.

Corresponding to the shock pattern of Figs. 5-7, Figs. 9-11 show the static pressure distribution along the top wall of the duct (the measurement along the bottom wall is confirmed to be almost identical to the one along the top). The gradual rise

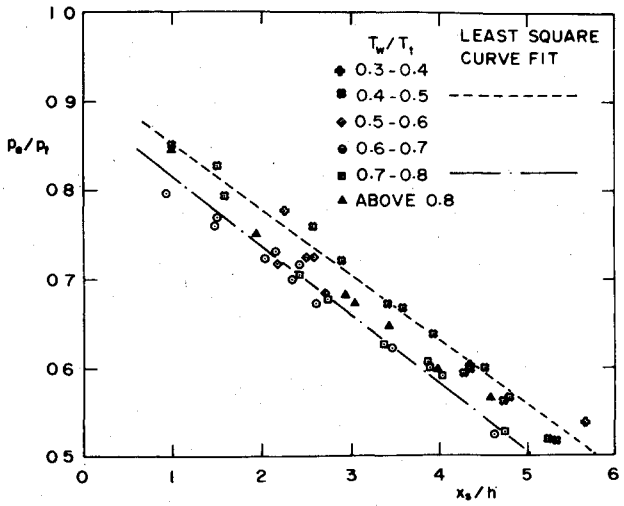


**Fig. 8 Relation of shock position with exhaust pressure and wall temperature.**

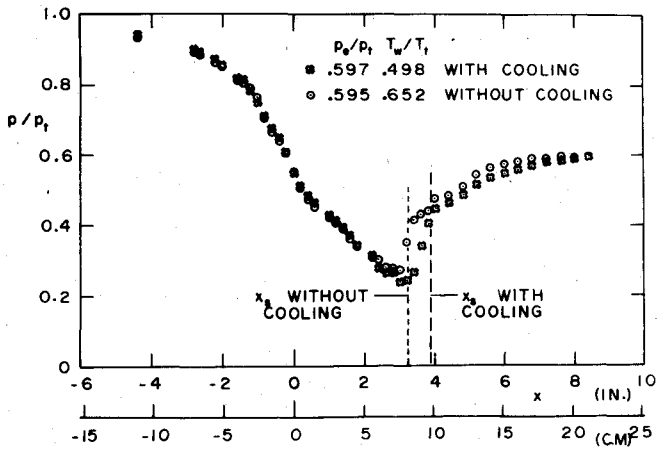


**Fig. 9 Pressure distribution corresponding to Fig. 5.**

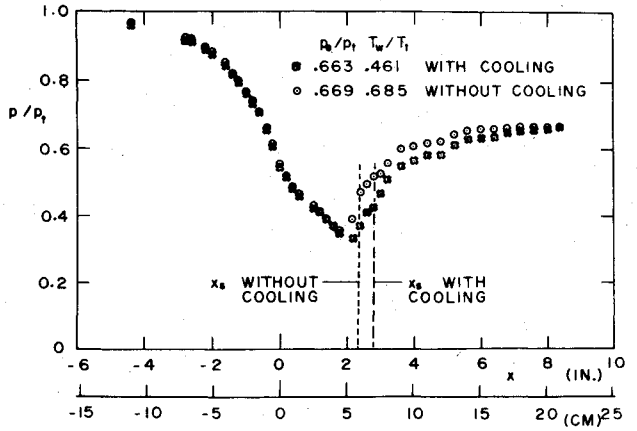


**Fig. 10 Pressure distribution corresponding to Fig. 6.**

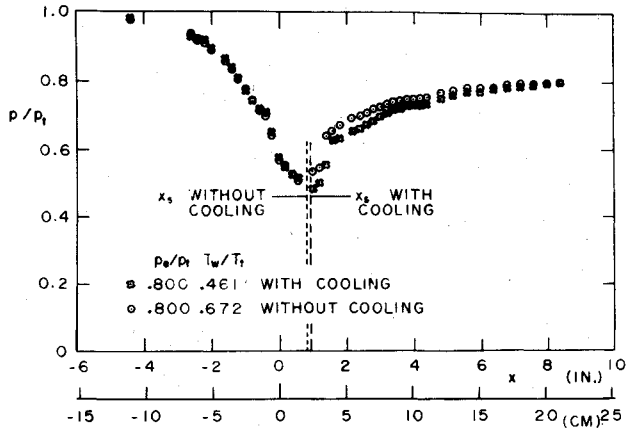


**Fig. 11 Pressure distribution corresponding to Fig. 7.**

of pressure across the shock is, of course, typical of the one through the bifurcated leg of the normal shock near the wall where the static pressure is measured. Notice that, although the pressure distribution upstream of the shock remains unaffected by the cooling, for the cooled wall the pressure immediately downstream of the shock is lower than that of the uncooled wall. This is observed to be so in Figs. 9 and 10 alike, where the shift in the shock position due to cooling is sizeable; such a difference disappears in Fig. 11, where the shock movement is now negligible. This yields an obvious clue to the physical explanation for the shift in the shock position, which will be discussed shortly.

## Discussion

Starting from a rudimentary viewpoint of one-dimensional inviscid flow treatment, the familiar shift in the sonic location due to heat transfer is given by[15]

$$dA/A = -dQ/c_pT \qquad (1)$$

where by cooling, the sonic line migrates upstream of the geometrical throat. For the present tests, $dQ/c_pT$ is approximately equal to $5\times10^{-3}$; therefore, the sonic line still remains virtually at the throat.

Before proceeding to the discussion of viscous effect, it is, of course, necessary to identify whether the flow is laminar or turbulent. In the present situation, the answer is not that straightforward, since the favorable pressure gradient, if sufficiently strong, is known to relaminarize the flow, even when the incoming flow is turbulent[16-19]; the wall cooling may exert additional stabilizing effect. To determine this, the boundary-layer traverse is carried out for hot and cold runs. Figure 12 shows the results in the usual "law of the wall" representation in terms of a frictional velocity $u_\tau$; this appears to show that the flow indeed remains turbulent. The reversion to laminar flow does not take place here because of the mild rate of pressure decrease, as indicated by the low value of an acceleration parameter $K=\mu_e/(\rho_e u_e^2)(du_e/dx)$, which is less than $1\times10^{-6}$ in the present test section. In addition to Fig. 12, the following circumstances serve to confirm the fact that the flow is always turbulent: 1) the lack of any noticeable change due to the boundary-layer trip installed upstream of the throat; 2) the presence of vigorous disturbances due to the combustion process; and 3) the agreement of hot-run data for oblique shock angles, corresponding to the bifurcated leg of the main shock, with the one based on Mager's[20,21] turbulent separation criterion.

Once the nature of the flow is confirmed to be turbulent and with the flow specified as such, an available computer code, a time-dependent Navier-Stokes equation solver developed by Cline,[22] is run for comparison. The results for an ideally expanded nozzle are shown in Fig. 13, both for cooled and thermally insulated walls. The pressure distribution stands in satisfactory agreement with the data for points upstream of the shock—this, of course, is the region where the comparison is meaningful; also, in that region, one observes that the effect of cooling is small, as seen in the experimental data. Although the difference is slight, the higher pressure for the cooled wall indicates that the displacement thickness $\delta^*$ for the cooled wall is thinner than the one for the insulated wall, as expected.

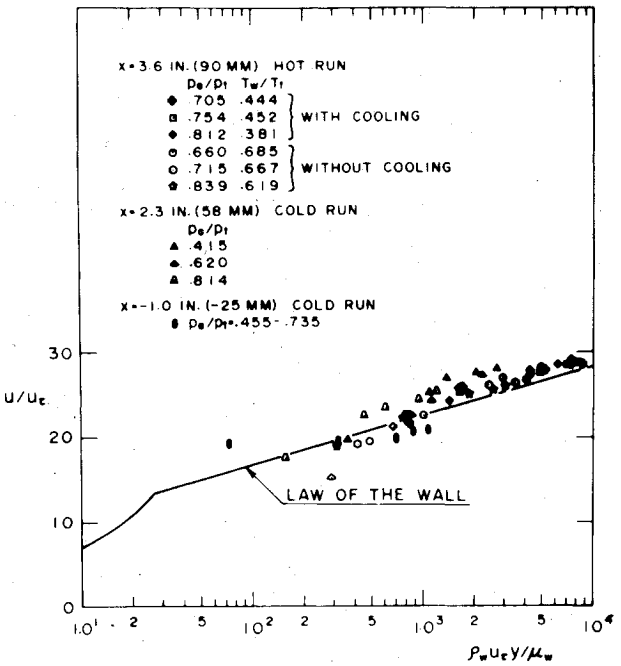


Fig. 12 Boundary-layer profile.

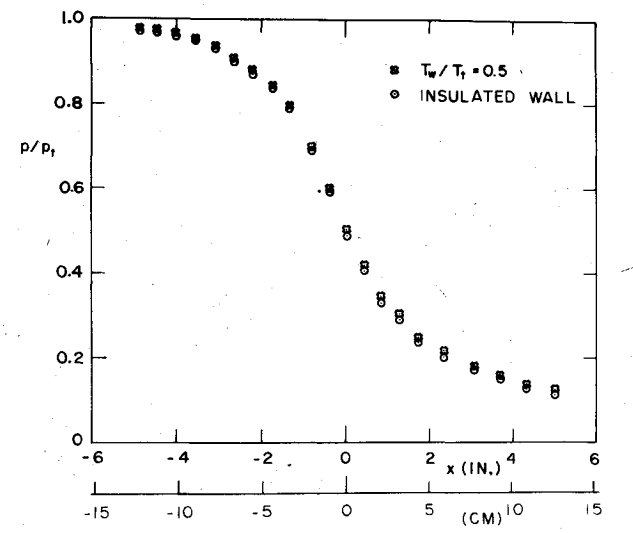


Fig. 13 Pressure distribution from Cline's turbulent code.

However, the difference of the displacement thickness between the cooled and the uncooled walls, although small upstream of the shock, becomes considerably magnified downstream of the shock. This is due to the separation and subsequent thickening of the boundary layer by the shock; this tends to amplify the difference between two displacement thicknesses, resulting in the sizeable change in the pressure distribution and shock position. Although no complete traverse of the boundary layer downstream of the shock has been obtained, data taken at $p_e/p_t \sim 0.7$ and $x = 91$ mm (3.6 in.) [this corresponds to the separation distance of 51 mm (2 in.) between the traverse station and the nominal position of the shock] are listed in Table 2; there, for comparison, the displacement thicknesses just upstream of the shock estimated from Cline's code are included. Observe the magnified difference between $\delta^*$ for cooled and uncooled walls downstream of the shock.

Figures 14a and 14b display this schematically: in the region downstream of the shock, the diffusion for the uncooled wall (Fig. 14b) is less than the one for the cooled wall (Fig. 14a).

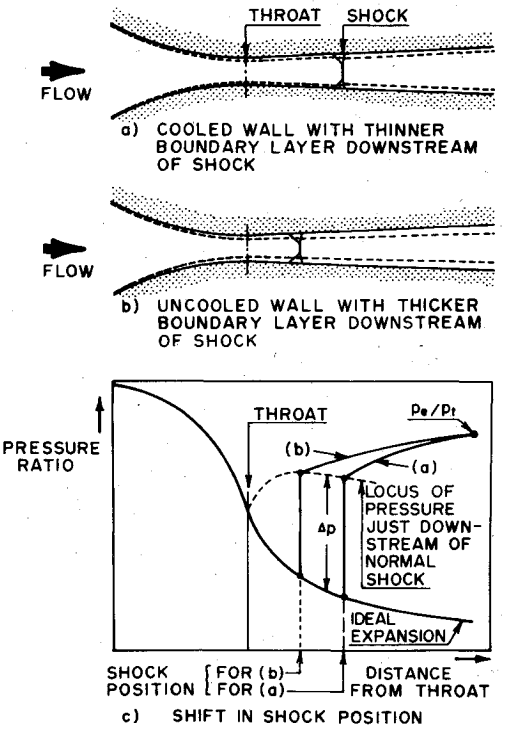


Fig. 14 Effect of cooling upon boundary-layer thickness downstream of shock.

Table 2 Displacement thicknesses

| Measured $\delta^*$ 51 mm (2.0 in.) downstream of shock | | Calculated $\delta_t^*$ just upstream of shock | |
|---|---|---|---|
| With cooling mm (in.) | Without cooling mm (in.) | With cooling mm (in.) | Without cooling (insulated wall) mm (in.) |
| 0.79 (0.031) | 1.55 (0.061) | 0.08 (0.003) | 0.10 (0.004) |

Consequently, for the same $p_e/p_t$, the pressure distribution downstream of the shock differs in the manner shown in Fig. 14c. When one adds the pressure rise across a normal shock to the ideally expanded curve and draws the locus of pressure just downstream of the shock (the dotted line), the intersection of this with the subsonic diffuser part of the pressure distribution determines the shock position; the position of the shock for the cooled wall is thus shifted in the downstream direction. It is also obvious why the amount of the shock movement becomes less as the shock approaches the throat; this reduces the pressure rise across the shock and hence the difference in the displacement thickness tends to disappear.

## Conclusion

It has been shown experimentally that in a convergent-divergent duct the position of the shock shifts downstream by the effect of wall cooling; for $T_w/T_t \sim 0.5$ and $p_e/p_t \sim 0.5$, not untypical values for the transonic turbine stator, the amount of the shock movement is found to be as large as 18 mm (0.7 in.).

## Acknowledgment

The authors express their gratitude to R. Ray for his able assistance for the entire phase of experiments; to Drs. J. E. Caruthers and W. H. Heiser for their valuable comments; to General Electric Company, Evendale, Ohio, for its donation

of J-79 combustors to The University of Tennessee Space Institute.

The work reported in this paper is supported by the NASA Lewis Research Center under NASA Grant 3487, with Dr. R. Siegel as a technical monitor. The valuable technical comments of Drs. Siegel and W. D. McNally, NASA Lewis Research Center, are gratefully acknowledged.

## References

[1] Gopalakrishnan, S. and Bozzola, R., "A Numerical Technique for the Calculation of Transonic Flows in Turbomachinery Cascades," ASME Paper 71-GT-40, 1971.

[2] Gopalakrishnan, S. and Bozzola, R., "Computation of Shocked Flows in Compressor Cascades," ASME Paper 72-GT-31, 1972.

[3] McDonald, P. W., "The Computation of Transonic Flow Through Two-Dimensional Gas Turbine Cascades," ASME Paper 71-GT-89, 1971.

[4] Delaney, R. A. and Kavanaugh, P., "Transonic Flow Analysis in Axial-Flow Turbomachinery Cascades by a Time-Dependent Method of Characteristics," *Transactions of the ASME,* Series A, *Journal of Engineering for Power,* Vol. 98, No. 3, 1976, pp. 356-364.

[5] Ives, D. C. and Liutermoza, J. F., "Analysis of Transonic Cascade Flow Using Conformal Mapping and Relaxation Techniques," *AIAA Journal,* Vol. 15, May 1977, pp. 647-652.

[6] Gliebe, P. R., "Coupled Inviscid/Boundary-Layer Flow Field Predictions for Transonic Turbomachinery Cascades," *Transonic Flow Problems in Turbomachinery,* edited by T. C. Adamson Jr. and M. F. Platzer, Hemisphere Publishing Corp., New York, 1976, pp. 434-453.

[7] Hartsel, J. E., "Prediction of Effects of Mass-Transfer Cooling on the Blade-Row Efficiency of Turbine Airfoils," AIAA Paper 72-11, 1972.

[8] Whitney, W. J., Szanca, E. M., Moffitt, T. P., and Monroe, D. E., "Cold Air Investigation of a Turbine for High-Temperature Engine Application, I: Turbine Design and Overall Stator Performance," NASA TN D-3751, 1967.

[9] Prust, H. W., Schum, H. J., and Behning, F. P., "Cold Air Investigation of a Turbine for High-Temperature Engine Application, II: Detailed Analytical and Experimental Investigation of Stator Performance," NASA TN D-4418, 1968.

[10] Whitney, W. J., Szanca, E. M., and Behning, F. P., "Cold Air Investigation of a Turbine with Stator-Blade Trailing-Edge Coolant Injection, I: Overall Stator Performance," NASA TM X-1901, 1969.

[11] Prust, H. W., Schum, H. J., and Szanca, E. M., "Cold Air Investigation of a Turbine with Transpiration-Cooled Stator Blades, I: Performance of Stator with Discrete Hole Blading," NASA TM X-2094, 1970.

[12] Behning, F. P., Prust, H. W., and Moffitt, T. P., "Cold Air Investigation of a Turbine with Transpiration-Cooled Stator Blades, III: Performance of Stator Blades with Wire-Mesh Shell Blading," NASA TM X-2166, 1971.

[13] Shapiro, A. H., "The Dynamics and Thermodynamics of Compressible Fluid Flow," Vol. 1, Ronald Press, New York, 1953, p. 231.

[14] Studerus, C. J., "Aerodynamics Effects of Surface Cooling-Flow Injection on Turbine Transonic Flow Fields," AIAA Paper 79-0048, 1979.

[15] Broadbent, E. G., "Flows with Heat Addition," *Progress in Aerospace Science,* Vol. 17, No. 2, 1976, pp. 93-100.

[16] Patel, V. C. and Head, M. R., "Reversion of Turbulent to Laminar Flow," *Journal of Fluid Mechanics,* Vol. 34, Pt. 2, 1968, pp. 371-392.

[17] Boldman, D. R., Schmidt, J. F., and Gallagher, A. K., "Laminarization of a Turbulent Boundary Layer as Observed from Heat Transfer and Boundary-Layer Measurements in Conical Nozzles," NASA TN D-4788, 1968.

[18] Boldman, D. R. and Graham, R. W., "Heat Transfer and Thermal Boundary Layer in a Conical Nozzle," AIAA Paper 69-474, 1969.

[19] Back, L. H., Cuffel, R. F., and Massier, P. F., "Laminarization of a Turbulent Boundary Layer in Nozzle-Flow, Boundary Layer and Heat Transfer Measurement with Wall Cooling," *Transactions of ASME, Series C, Journal of Heat Transfer,* Vol. 92, Aug. 1970, pp. 333-344.

[20] Mager, A., "Prediction of Shock-Induced Turbulent Boundary Layer Separation," *Journal of the Aeronautical Sciences,* Vol. 22, No. 3, 1955, pp. 201-202.

[21] Sehgal, R. and Wu, J. M., "Thrust Vector Control by Liquid Injection into Rocket Nozzles," *Journal of Spacecraft and Rockets,* Vol. 1, Sept.-Oct. 1964, pp. 545-551.

[22] Cline, M. C., "VNAP: A Computer Program for Computation of Two-Dimensional, Time-Dependent Compressible, Viscous Internal Flow," Los Alamos Scientific Laboratory Rept. LA-7326, University of California, 1978.